Mechanical Systems and Signal Processing 99 (2018) 434–449

Contents lists available at ScienceDirect

Mechanical Systems and Signal Processing

journal homepage: www.elsevier.com/locate/ymssp

Fuzzy adaptive integration scheme for low-cost SINS/GPS navigation system

Hossein Nourmohammadi, Jafar Keighobadi *

Department of Mechanical Engineering, University of Tabriz, Tabriz, Iran

ARTICLE INFO

Article history:
Received 27 August 2016
Received in revised form 21 April 2017
Accepted 23 June 2017

Keywords:
Low-cost SINS/GPS
Fuzzy adaptive integration
Orientation estimation
Long-term navigation error
State estimation

ABSTRACT

Due to weak stand-alone accuracy as well as poor run-to-run stability of micro-electro mechanical system (MEMS)-based inertial sensors, special approaches are required to integrate low-cost strap-down inertial navigation system (SINS) with global positioning system (GPS), particularly in long-term applications. This paper aims to enhance long-term performance of conventional SINS/GPS navigation systems using a fuzzy adaptive integration scheme. The main concept behind the proposed adaptive integration is the good performance of attitude-heading reference system (AHRS) in low-accelerated motions and its degradation in maneuvered or accelerated motions. Depending on vehicle maneuvers, gravity-based attitude angles can be intelligently utilized to improve orientation estimation in the SINS. Knowledge-based fuzzy inference system is developed for decision-making between the AHRS and the SINS according to vehicle maneuvering conditions. Inertial measurements are the main input data of the fuzzy system to determine the maneuvering level during the vehicle motions. Accordingly, appropriate weighting coefficients are produced to combine the SINS/GPS and the AHRS, efficiently. The assessment of the proposed integrated navigation system is conducted via real data in airborne tests.

1. Introduction

Advances in micro-electro mechanical system (MEMS) technologies have led to significant developments in low-cost strap-down inertial navigation systems (SINSs). When cost or weight is an important issue in application of navigation systems, heavy accurate inertial sensors are excluded and instead, low-cost systems like MEMS-grade gyroscopes and accelerometers are proposed. However, by use of the current generation of low-cost inertial measurement units (IMUs), the navigation error of stand-alone SINS intensively increases over time owing to sensor noise, bias and drift of the MEMS-grade IMUs [1]. The global positioning system (GPS) and the SINS have very complementary characteristics. As the main benefit of gathered GPS receiver with a SINS, online calibration of the SINS sensors is performed through the GPS absolute and drift-free measurements. On the other hand, the low frequency 1 (up to 20) Hz update rate of GPS data are compensated by the high frequency SINS to provide accurate position and orientation data at high update rate [2]. SINS is a self-contained unit which provides position, velocity and orientation regardless of external environment. In contrary, the GPS performance depends on external environment and satellite accessibility. Hence, the above-mentioned complementary characteristics motivate the design of integrated SINS/GPS navigation system to obtain combined superior performance with respect to the individual subsystems SINS and GPS.

* Corresponding author at: 29 Bahman, P.C. 5166614766, Tabriz, Iran.
E-mail address: keighobadi@tabrizu.ac.ir (J. Keighobadi).

http://dx.doi.org/10.1016/j.ymssp.2017.06.030
0888-3270/

Several documented researches can be addressed in the literature concerning integrated navigation systems. For example, Kubo et al. proposed combination algorithms of INS/GPS based on nonlinear techniques comprising quasi-linear optimal filter and Gaussian-sum filter [3]. Wang et al. proposed a quadratic extended Kalman filter for INS/GPS integration by considering the second-order terms of Taylor approximation of nonlinear INS dynamics in propagation of estimation covariance matrix [4]. A nonlinear sliding-mode observer has been proposed for a low-cost attitude-heading reference system (AHRS) [5]. Using infinite impulse response (IIR) digital low-pass filter, a new algorithm for initial alignment of marine SINS has been developed in [6]. Magnetic calibration of strap-down magnetometers for the INS heading angle correction has been conducted in [7]. Jaradat and Abdel-Hafez proposed auto-regressive neural network-based data fusion architecture for the integration between low-cost INS and GPS systems [8]. Nourmohamadi and Keighobadi developed a direct decentralized integration scheme for low-cost INS/GPS system in which QR-factorized cubature Kalman filter has been used as the state estimation algorithm [9].

In practical applications, particularly in aerospace engineering, orientation estimation accuracy is an important challenge of low-cost SINS/GPS systems. Some valuable efforts have been conducted to enhance the performance of the integrated inertial navigation systems. However, most of the documented researches merely concentrated on data fusion and state estimation algorithms. Therefore, as the main topic of the proposed research work, the adaptive combination of the SINS/GPS and the AHRS is considered to take advantages of both systems simultaneously. Considering this fact, in this paper an adaptive integration scheme is presented based on fuzzy logic. Unlike crisp sets, fuzzy sets allow partial membership assignment which means that an element may partially belong to more than one set. Therefore, fuzzy logic-based algorithms are much closer in spirit to human thinking than the traditional Aristotelian logical systems [10]. Nowadays, fuzzy logic has become a powerful tool for optimizing the performance of many practical systems, especially in the field of estimation and control [11–16]. For example, Petkovic et al. used adaptive neuro-fuzzy inference system (ANFIS) to estimate optimal power coefficient value of wind turbines [14]. Musavi and Keighobadi proposed an adaptive fuzzy neuro-observer to enhance the performance of integrated INS/GPS positioning systems [15]. Boada et al. proposed a new observer using fuzzy inference system in combination with an unscented Kalman filter which enhanced the estimation accuracy of vehicle sideslip angle [16].

In the current research work, through intelligent fuzzy implications an adaptive integration scheme is developed for SINS/GPS navigation system. Using knowledge-based Mamdani-type fuzzy inference, the inertial measurements comprising gyroscopes and accelerometers outputs are examined to detect the maneuvering level of the vehicle. Accordingly, appropriate weighting coefficients are obtained to combine the SINS/GPS and the AHRS, efficiently. In low-accelerated intervals of motion, the AHRS algorithm data take larger weighting coefficients. However, when the vehicle undergoes non-gravitational accelerations, the orientation results will mostly tend to get the SINS data.

The long-term performance of the proposed approach is assessed through real field test. Low-cost ADIS-16407 IMU is used as the MEMS-grade inertial sensors and the measurement data of the estimation algorithm is provided through Garmin-35 GPS receiver. Furthermore, highly accurate Vitans navigation system is used to produce the reference data for evaluation.

2. Integrated SINS/GPS navigation

This section deals with developing a fifteen-state SINS/GPS navigation algorithm. Following deriving dynamics of the SINS error, the appropriate estimation filter is designed to integrate the SINS with the GPS, efficiently. Fifteen states of error dynamics system include five triple sets of misalignment error, velocity error, position error, accelerometer bias and gyroscope drift components. The measurement vector of integration filter is constituted by the GPS position, velocity and heading angle.

2.1. SINS dynamics

A strap-down inertial system benefits a major hardware simplification of the old stable-platform navigation systems. Strap-down navigation overcomes the problems encountered with the stable-platform navigation systems, and most importantly reduces the size, cost and power consumption [17]. Several reference frames are used in the inertial navigation comprising of inertial frame (i-frame), Earth-fixed frame (e-frame), navigation frame (n-frame) and body frame (b-frame). In the paper, the coordinate frames are defined based on Fig. 1.

Here, the n-frame is considered the local level navigation frame with north-east-down (NED) geodetic axes. Dynamical equations of the SINS position, velocity and orientation components are summarized as follows [18].

$$\begin{aligned}
&\dot{L} = \frac{v_N}{R_N + h}, \quad \dot{l} = \frac{v_E}{(R_E + h)\cos L}, \quad \dot{h} = -v_D \\
&\dot{\boldsymbol{v}}^n = \boldsymbol{C}_b^n \boldsymbol{f}^b - (2\boldsymbol{\omega}_{ie}^n + \boldsymbol{\omega}_{en}^n) \times \boldsymbol{v}^n + \boldsymbol{g}^n \\
&\dot{\boldsymbol{C}}_b^n = \boldsymbol{C}_b^n \boldsymbol{\Omega}_{nb}^b
\end{aligned} \tag{1}$$

where L, l and h are the position coordinates comprising latitude, longitude and altitude; $\boldsymbol{v}^n = [v_N \; v_E \; v_D]^T$ stands for the velocity vector represented in the n-frame, $\boldsymbol{C}_b^n$ is the direction cosine matrix (DCM) from b-frame to the n-frame; $\boldsymbol{f}^b$ is the specific force measured by the accelerometers in b-frame and $\boldsymbol{g}^n = [0\; 0\; g]^T$ is the gravity vector in the n-frame. R_N and R_E

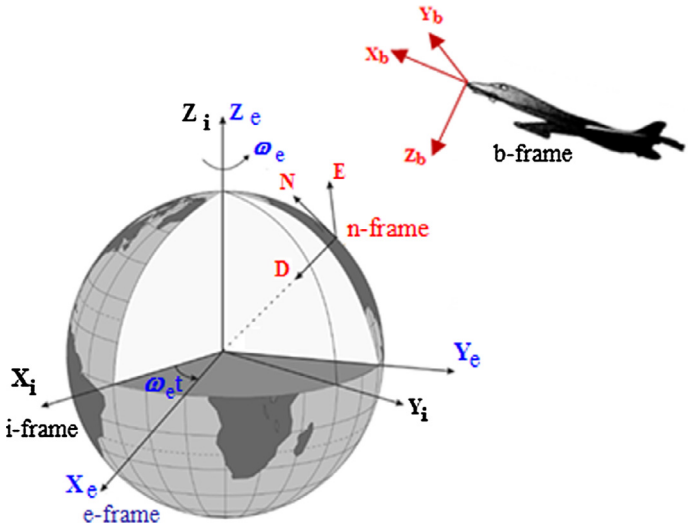

Fig. 1. Reference coordinates frames in inertial navigation systems.

represent meridian radii of curvature and transverse radii of curvature, respectively [18]. The Earth rate, $\boldsymbol{\omega}_{ie}^{n}$ and the rate of the n-frame with respect to the e-frame, $\boldsymbol{\omega}_{en}^{n}$ are explained as follows.

$$\begin{aligned}\boldsymbol{\omega}_{ie}^{n} &= [\,\omega_e cosL \quad 0 \quad -\omega_e sinL\,]^T \\ \boldsymbol{\omega}_{en}^{n} &= \left[\,\dot{l}cosL \quad -\dot{L} \quad -\dot{l}sinL\,\right]^T\end{aligned} \tag{2}$$

where ω_e is the magnitude of the Earth rotation rate. The skew-symmetric matrix, $\boldsymbol{\Omega}_{nb}^{b}$ of vector $\boldsymbol{\omega}_{nb}^{b}$ represents the rotation rate of the vehicle b-frame with respect to the n-frame. $\boldsymbol{\omega}_{nb}^{b}$ is obtained as:

$$\boldsymbol{\omega}_{nb}^{b} = \boldsymbol{\omega}_{ib}^{b} - \boldsymbol{C}_{n}^{b}[\boldsymbol{\omega}_{ie}^{n} + \boldsymbol{\omega}_{en}^{n}] \tag{3}$$

$\boldsymbol{\omega}_{ib}^{b}$ stands for the measured angular rate vector by gyroscopes. The orientation coordinates are defined by Euler angles including roll angle, φ about body x-axis, pitch angle, θ about y-axis and yaw angle, ψ about z-axis. Considering the z-y-x order of rotations, the DCM matrix between the b-frame and the n-frame is defined as:

$$\boldsymbol{C}_{b}^{n} = \begin{bmatrix} C\theta C\psi & -C\varphi S\psi + S\varphi S\theta C\psi & S\varphi S\psi + C\varphi S\theta C\psi \\ C\theta S\psi & C\varphi C\psi + S\varphi S\theta S\psi & -S\varphi C\psi + C\varphi S\theta S\psi \\ -S\theta & S\varphi C\theta & C\varphi C\theta \end{bmatrix} \tag{4}$$

where C and S stand for cosine and sine functions, respectively. Now, using (1) through (4) together with the given initial alignment states and the IMU measurements, the navigation output data can be computed. However, due to the large noise and bias of MEMS-grade sensors of IMU, the navigation error of the stand-alone SINS is quickly increased over time.

The navigation error in a strap-down inertial navigation algorithm mostly arises from inaccurate measurements by the MEMS-grade IMU. The inaccurately measured accelerations in the b-frame are transformed into the n-frame through the erroneous computations of the orientation and the DCM matrix. Mutually, the computational error of navigation states will be propagated into the computation of rotation rates, $\boldsymbol{\omega}_{ie}^{n}$ and $\boldsymbol{\omega}_{en}^{n}$. Therefore, the three-time integration of gyroscope drift and two-time integration of accelerometer bias lead to time increasing errors of computed position coordinates. The standard form of the SINS error model is organized based on dynamics of three error vectors including position, velocity and misalignment errors. The linearized error model of the SINS is obtained by perturbing the SINS dynamical equations. Considering the very small time interval between the measurement updates, the linear propagation model of the SINS error satisfies the required accuracy. The position and velocity vectors errors are defined as:

$$\begin{aligned}\delta\boldsymbol{r} &= \hat{\boldsymbol{r}} - \boldsymbol{r} = [\,\delta L \quad \delta l \quad \delta h\,]^T \\ \delta\boldsymbol{v}^{n} &= \hat{\boldsymbol{v}}^{n} - \boldsymbol{v}^{n} = [\,\delta v_N \quad \delta v_E \quad \delta v_D\,]^T\end{aligned} \tag{5}$$

Note that, ^ specifies the estimated values. Based on Poisson equation, the estimated DCM matrix, $\hat{\boldsymbol{C}}_{b}^{n}$ is written in terms of the true DCM matrix, $\boldsymbol{C}_{b}^{n}$ and the misalignment errors as follows [18].

$$\hat{\boldsymbol{C}}_{b}^{n} = [\boldsymbol{I} - \boldsymbol{E}]\boldsymbol{C}_{b}^{n} \tag{6}$$

where $\boldsymbol{I}$ is identity matrix and $\boldsymbol{E}$ represents skew-symmetric misalignment matrix constructed by the misalignment angles vector, $\boldsymbol{\varepsilon}$ with components, $\delta\alpha$, $\delta\beta$ and $\delta\gamma$ as:

$$\boldsymbol{E} = [\boldsymbol{\varepsilon}\times] = \begin{bmatrix} 0 & -\delta\gamma & \delta\beta \\ \delta\gamma & 0 & -\delta\alpha \\ -\delta\beta & \delta\alpha & 0 \end{bmatrix} \tag{7}$$

By use of small variation approach in linearization of the SINS dynamics model in Eq. (1), the following error dynamics is obtained.

$$\begin{aligned} \delta\dot{L} &= \tfrac{-v_N}{(R_N+h)^2}\delta h + \tfrac{1}{R_N+h}\delta v_N \\ \delta\dot{l} &= \tfrac{v_E \sin L}{(R_E+h)\cos^2 L}\delta L + \tfrac{-v_E}{(R_E+h)^2\cos L}\delta h + \tfrac{1}{(R_E+h)\cos L}\delta v_E \\ \delta\dot{h} &= -\delta v_D \end{aligned} \tag{8}$$

$$\begin{aligned} \delta\dot{v}_N = {} & -f_D\delta\beta + f_E\delta\gamma + \frac{v_D}{R_N+h}\delta v_N - 2\sin L\left(\omega_e + \frac{v_E}{(R_E+h)\cos L}\right)\delta v_E + \frac{v_N}{R_N+h}\delta v_D \\ & - \left(2\omega_e v_E \cos L + \frac{v_E^2}{(R_E+h)\cos^2 L}\right)\delta L + \left(\frac{v_E^2 \tan L}{(R_E+h)^2} - \frac{v_N v_D}{(R_N+h)^2}\right)\delta h + B_N \end{aligned} \tag{9-1}$$

$$\begin{aligned} \delta\dot{v}_E = {} & f_D\delta\alpha - f_N\delta\gamma + \left(2\omega_e \sin L + \frac{v_E \tan L}{R_E+h}\right)\delta v_N + \left(\frac{v_D + v_N \tan L}{R_E+h}\right)\delta v_E + \left(2\omega_e \cos L + \frac{v_E}{R_E+h}\right)\delta v_D \\ & + \left(2\omega_e(v_N \cos L - v_D \sin L) + \frac{v_N v_E}{(R_E+h)\cos^2 L}\right)\delta L - \left(\frac{v_E(v_D + v_N \tan L)}{(R_E+h)^2}\right)\delta h + B_E \end{aligned} \tag{9-2}$$

$$\begin{aligned} \delta\dot{v}_D = {} & -f_E\delta\alpha + f_N\delta\beta - \frac{2v_N}{R_N+h}\delta v_N - 2\left(\omega_e \cos L + \frac{v_E}{R_E+h}\right)\delta v_E + 2\omega_e v_E \sin L\delta L \\ & + \left(\frac{v_E^2}{(R_E+h)^2} + \frac{v_N^2}{(R_N+h)^2} - \frac{2g}{R+h}\right)\delta h + B_D \end{aligned} \tag{9-3}$$

$$\begin{aligned} \delta\dot{\alpha} &= -\left(\omega_e \sin L + \tfrac{v_E \tan L}{R_E+h}\right)\delta\beta + \tfrac{v_N}{R_N+h}\delta\gamma + \tfrac{1}{R_E+h}\delta v_E - \omega_e \sin L\delta L - \tfrac{v_E}{(R_E+h)^2}\delta h - D_N \\ \delta\dot{\beta} &= \left(\omega_e \sin L + \tfrac{v_E \tan L}{R_E+h}\right)\delta\alpha + \left(\omega_e \cos L + \tfrac{v_E}{R_E+h}\right)\delta\gamma - \tfrac{1}{R_N+h}\delta v_N + \tfrac{v_N}{(R_N+h)^2}\delta h - D_E \\ \delta\dot{\gamma} &= -\tfrac{v_N}{R_N+h}\delta\alpha - \left(\omega_e \cos L + \tfrac{v_E}{R_E+h}\right)\delta\beta - \tfrac{\tan L}{R_E+h}\delta v_E - \left(\omega_e \cos L + \tfrac{v_E}{(R_E+h)\cos^2 L}\right)\delta L + \tfrac{v_E \tan L}{(R_E+h)^2}\delta h - D_D \end{aligned} \tag{10}$$

where $\boldsymbol{f}^n = [f_N\, f_E\, f_D]^T$ represents the specific force vector in the n-frame. $\boldsymbol{B} = [B_N\, B_E\, B_D]^T$ and $\boldsymbol{D} = [D_N\, D_E\, D_D]^T$ are the accelerometers bias and gyroscopes drift vector projected in the n-frame, respectively. To represent the orientation angles errors in terms of misalignment error angles of Eq. (7), first the components of estimated DCM matrix are expanded in terms of the trigonometric relationships for sums of angles. Next, the resulted terms are equated with their corresponding terms from the matrix multiplication given by Eq. (6) which yields:

$$\begin{bmatrix} \delta\varphi \\ \delta\theta \\ \delta\psi \end{bmatrix} = \begin{bmatrix} -cos\psi sec\theta & -sin\psi sec\theta & 0 \\ sin\psi & -cos\psi & 0 \\ -tan\theta cos\psi & -tan\theta sin\psi & -1 \end{bmatrix} \begin{bmatrix} \delta\alpha \\ \delta\beta \\ \delta\gamma \end{bmatrix} \tag{11}$$

IMU inaccuracies deteriorate the overall navigation accuracy of the SINS. Compared with accelerometer errors, the gyroscope errors have more effects on the SINS performance. To this end, the errors of IMU accelerometers and gyroscopes are modeled and included in the SINS error model. The IMU error terms are commonly adopted with the gyroscope drift approximated by first order Gauss-Markov process and the accelerometer bias as a fixed value. Therefore, the gyroscope drift and the accelerometer bias are modeled as follows [19].

$$\begin{aligned} \dot{D}_i &= -\beta D_i + \sigma\sqrt{2\beta}w(t), \quad i = N, E, D \\ \dot{B}_i &= 0, \quad i = N, E, D \end{aligned} \tag{12}$$

where β and σ denote the correlation coefficient and the standard deviation of the sensor measurement, respectively; and $w(t)$ represents Gaussian white noise with unity power spectral density. It should be mentioned that Gauss-Markov

Table 1
Comparison between the SINS and the GPS characteristics.

Properties	SINS	GPS
Sampling rate	High (1–1000 Hz)	Low (1–20 Hz)
Short-term accuracy	High	High
Long-term accuracy	Low	High
Independence	Self-contained	Depended on environments
Attitude measurement	Compact and reliable	Only for heading angle
Continuous navigation	Yes	No

coefficients can be determined from stationary data of the sensor after removing the mean value of the data over a specific time interval.

2.2. Integration scheme

Table 1 describes a brief comparison between the SINS ant the GPS characteristics. It can be obviously inferred from Table 1 that there are very complementary characteristics between the SINS and GPS specifications. The complementary characteristics motivate the implementation of combined SINS/GPS navigation system through suitable integration filters. As the most commonly used estimation algorithm for integration of SINS/GPS, Kalman filter and its extended version yield good results among white noisy observations.

In this section, fifteen-state SINS/GPS integration scheme is developed based on SINS error dynamics. The state vector is defined as follow.

$$\boldsymbol{x} = [\delta a\ \delta\beta\ \delta\gamma\ \delta v_N\ \delta v_E\ \delta v_D\ \delta L\ \delta l\ \delta h\ B_N\ B_E\ B_D\ D_N\ D_E\ D_D]^T \tag{13}$$

The system dynamics can be expressed in accordance with the following state-space model.

$$\dot{\boldsymbol{x}} = \boldsymbol{A}\boldsymbol{x} + \boldsymbol{G}\boldsymbol{u} \tag{14}$$

The matrix $\boldsymbol{A}$ is determined based on the SINS error dynamics explained in Eqs. (8)–(10) and (12). The design weighting matrix of uncertainties, $\boldsymbol{G}$ is considered the distribution matrix of process white noise vector, $\boldsymbol{u}$ gathered with 10% extra modelling uncertainty. The SINS is usually implemented with high-rate sampled data in high performance digital microprocessors. Therefore, Eq. (14) is transformed into its discrete-time form as follows.

$$\boldsymbol{x}_{k+1} = \boldsymbol{\Phi}_k \boldsymbol{x}_k + \boldsymbol{w}_k \tag{15}$$

where $\boldsymbol{\Phi}_k$ is the state transition matrix, and $\boldsymbol{w}_k$ is the driven response at time t_{k+1} due to the system noise during the short time interval (t_k, t_{k+1}). Since a white sequence is constituted by zero-mean random variables which are uncorrelated time-wise, the covariance matrix associated with $\boldsymbol{w}_k$ is defined as:

$$E[\boldsymbol{w}_k \boldsymbol{w}_i] = \begin{cases} \boldsymbol{Q}_k, & i = k \\ 0, & i \neq k \end{cases} \tag{16}$$

Similarly, the measurement equation is defined in accordance with the following discrete vector:

$$\boldsymbol{z}_k = \boldsymbol{H}_k \boldsymbol{x}_k + \boldsymbol{e}_k \tag{17}$$

where $\boldsymbol{H}_k$ is the observation matrix and $\boldsymbol{e}_k$ stands for the measurement noise with the following covariance matrix.

$$\begin{aligned} &E[\boldsymbol{e}_k \boldsymbol{e}_i] = \begin{cases} \boldsymbol{R}_k, & i = k \\ 0, & i \neq k \end{cases} \\ &E[\boldsymbol{w}_k \boldsymbol{e}_i] = 0, \quad \forall i, k \end{aligned} \tag{18}$$

The measurement vector is constructed by the error between the SINS and GPS position, velocity and finally the heading angle as follows.

$$\mathbf{z} = \begin{bmatrix} L^{INS} - L^G \\ l^{INS} - l^G \\ h^{INS} - h^G \\ v_N^{INS} - v_N^G \\ v_E^{INS} - v_E^G \\ v_D^{INS} - v_D^G \\ \psi^{INS} - \psi^G \end{bmatrix} \tag{19}$$

Accordingly, the observation matrix, $\boldsymbol{H}$ is obtained as:

$$\boldsymbol{H}=\begin{bmatrix}0&0&0&0&0&0&1&0&0&0&0&0&0&0&0\\0&0&0&0&0&0&0&1&0&0&0&0&0&0&0\\0&0&0&0&0&0&0&0&1&0&0&0&0&0&0\\0&0&0&1&0&0&0&0&0&0&0&0&0&0&0\\0&0&0&0&1&0&0&0&0&0&0&0&0&0&0\\0&0&0&0&0&1&0&0&0&0&0&0&0&0&0\\0&0&-1&0&0&0&0&0&0&0&0&0&0&0&0\end{bmatrix} \tag{20}$$

Kalman filter is applied as the estimation algorithm for the integration between the measurement data of Eq. (19) and the dynamics system of Eq. (14). The filter is implemented in two steps known as time update and measurement update [20]. Time update is the prediction stage in which the predicted values of the state vector, $\hat{\boldsymbol{x}}_k^-$ and the error covariance matrix, $\boldsymbol{P}_k^-$ are provided as:

$$\begin{aligned}\boldsymbol{P}_k^- &= \boldsymbol{\Phi}_{k-1}\boldsymbol{P}_{k-1}\boldsymbol{\Phi}_{k-1}^T+\boldsymbol{Q}_{k-1}\\ \hat{\boldsymbol{x}}_k^- &= \boldsymbol{\Phi}_{k-1}\hat{\boldsymbol{x}}_{k-1}\end{aligned} \tag{21}$$

Measurement update is the correction stage in which first the Kalman gain matrix, $\boldsymbol{K}_k$ is computed. Afterward, the state vector and the error covariance matrix are updated as follows.

$$\begin{aligned}\boldsymbol{K}_k &= \boldsymbol{P}_k^-\boldsymbol{H}_k^T\left(\boldsymbol{H}_k\boldsymbol{P}_k^-\boldsymbol{H}_k^T+\boldsymbol{R}_k\right)^{-1}\\ \hat{\boldsymbol{x}}_k &= \hat{\boldsymbol{x}}_k^-+\boldsymbol{K}_k\left(\mathbf{z_k}-\mathbf{H_k}\hat{\mathbf{x}}_\mathbf{k}^-\right)\\ \boldsymbol{P}_k &= (\boldsymbol{I}-\boldsymbol{K}_k\boldsymbol{H}_k)\boldsymbol{P}_k^-\end{aligned} \tag{22}$$

Finally, the position and the velocity components are corrected using the estimated position error and velocity error as:

$$L^C=L^{INS}-\delta\hat{L},\quad l^C=l^{INS}-\delta\hat{l},\quad h^C=h^{INS}-\delta\hat{h} \tag{23}$$

$$v_N^C=v_N^{INS}-\delta\hat{v}_N,\quad v_E^C=v_E^{INS}-\delta\hat{v}_E,\quad v_E^C=v_E^{INS}-\delta\hat{v}_E \tag{24}$$

where $\delta\hat{L}$, $\delta\hat{l}$ and $\delta\hat{h}$ are the Kalman filter's outputs for position error vector and similarly, $\delta\hat{v}_N$, $\delta\hat{v}_E$ and $\delta\hat{v}_D$ are the estimated velocity error. Moreover, using the estimated misalignment errors, the DCM matrix is corrected by rearranging Eq. (6) as follows.

$$\boldsymbol{C}_b^n=[\boldsymbol{I}+\boldsymbol{E}]\hat{\boldsymbol{C}}_b^n \tag{25}$$

Therefore, in-motion alignment is carried out during the navigation process and the corrected orientation can be calculated from the corrected DCM matrix by Eq. (11).

3. AHRS navigation system

A typical AHRS consists of three-axis gyroscopes, accelerometers and in some cases, a magnetometer. Using transformation algorithm, the angular rates in the navigation reference frame can be calculated from the gyroscope outputs. The attitude including the roll and pitch angles and the heading/yaw angle about body z-axis are obtained through time-integration of the angular rates. However, the gyro-based orientation is degraded by the time-growing errors caused by the gyroscope drift and the cumulative computation error. This section deals with design of a suitable state estimation algorithm to correct the gyro-based orientation using the measurements provided by the accelerometer and the GPS.

3.1. Orientation dynamics

Here, quaternion formulation is used to describe the dynamics model of the orientation of the AHRS algorithm. The quaternion is a four-component representation based on the idea that a transformation from one coordinate frame to another may be accomplished by a single rotation about a specific direction vector. The quaternion propagation with time is given in accordance with the following matrix form [21].

$$\begin{bmatrix}\dot{q}_0\\ \dot{q}_1\\ \dot{q}_2\\ \dot{q}_3\end{bmatrix}=\frac{1}{2}\begin{bmatrix}0&-\omega_x&-\omega_y&-\omega_z\\ \omega_x&0&\omega_z&-\omega_y\\ \omega_y&-\omega_z&0&\omega_x\\ \omega_z&\omega_y&-\omega_x&0\end{bmatrix}\begin{bmatrix}q_0\\ q_1\\ q_2\\ q_3\end{bmatrix} \tag{26}$$

where q_0, q_1, q_2 and q_3 denote the quaternion components. In Eq. (26), ω_x, ω_y and ω_z are the components of the vector $\boldsymbol{\omega}_{nb}^b$. In low-cost SINS, $\boldsymbol{\omega}_{nb}^b$ can be approximated into $\boldsymbol{\omega}_{ib}^b$ which is measured by the gyroscopes in the b-frame. The quaternion norm is equal to 1 and its components can be expressed in terms of the Euler angles as follows [21].

$$\begin{aligned} q_0 &= \cos\tfrac{\varphi}{2}\cos\tfrac{\theta}{2}\cos\tfrac{\psi}{2} + \sin\tfrac{\varphi}{2}\sin\tfrac{\theta}{2}\sin\tfrac{\psi}{2} \\ q_1 &= \sin\tfrac{\varphi}{2}\cos\tfrac{\theta}{2}\cos\tfrac{\psi}{2} - \cos\tfrac{\varphi}{2}\sin\tfrac{\theta}{2}\sin\tfrac{\psi}{2} \\ q_2 &= \cos\tfrac{\varphi}{2}\sin\tfrac{\theta}{2}\cos\tfrac{\psi}{2} + \sin\tfrac{\varphi}{2}\cos\tfrac{\theta}{2}\sin\tfrac{\psi}{2} \\ q_3 &= \cos\tfrac{\varphi}{2}\cos\tfrac{\theta}{2}\sin\tfrac{\psi}{2} - \sin\tfrac{\varphi}{2}\sin\tfrac{\theta}{2}\cos\tfrac{\psi}{2} \end{aligned} \tag{27}$$

Additionally, the DCM matrix is written in terms of quaternion components in accordance with the following equation [21].

$$\boldsymbol{C}_b^n = \begin{bmatrix} q_0^2+q_1^2-q_2^2-q_3^2 & 2(q_1q_2-q_0q_3) & 2(q_1q_3+q_0q_2) \\ 2(q_1q_2+q_0q_3) & q_0^2-q_1^2+q_2^2-q_3^2 & 2(q_2q_3-q_0q_1) \\ 2(q_1q_3-q_0q_2) & 2(q_2q_3+q_0q_1) & q_0^2-q_1^2-q_2^2+q_3^2 \end{bmatrix} \tag{28}$$

By imposing time-integration on Eq. (26), quaternion is continually updated. The DCM matrix associating with the updated quaternion is calculated in accordance with Eq. (28). Finally, the updated Euler angles can be obtained from the DCM matrix of Eq. (4).

3.2. Integration scheme

Due to the large drift of MEMS-grade gyroscopes, the orientation error in gyro-based AHRS grows up, quickly. To overcome this drawback, accelerometer outputs are integrated properly with gyro-based AHRS data. The roll and pitch angles computed by gravity matching of accelerometers output, provide the attitude measurements without long-term drift errors. However, it should be noticed that the gravity-based attitude determination would become inaccurate when the vehicle undergoes non-gravitational accelerations. Therefore, the vehicle maneuvering condition should be detected properly prior to use of the gravitational attitude as measurement data. Besides, the gravity field vector of the earth is perpendicular to the North axis which makes the heading angle undetectable in gravity vector matching between body and reference NED coordinate frames. Hence, GPS course angle is considered as measurement data of heading angle in the AHRS. In this section, an integration scheme of seven-state AHRS is developed based on quaternion equations. Dynamics system contains four quaternion components and three gyroscope drift components. The gravity matching attitude angles and the GPS heading angle constitute the measurement vector components. Therefore, the state vector is defined as follows.

$$\boldsymbol{x}^{ah} = \begin{bmatrix} q_0 & q_1 & q_2 & q_3 & D_x & D_y & D_z \end{bmatrix}^T \tag{29}$$

where D_x, D_y and D_z stand for the gyroscope drift components along the b-frame x-y-z axes. Adding the drift components on Eq. (26) results in:

$$\begin{bmatrix} \dot{q}_0 \\ \dot{q}_1 \\ \dot{q}_2 \\ \dot{q}_3 \end{bmatrix} = \frac{1}{2}\begin{bmatrix} 0 & -(\omega_x - D_x) & -(\omega_y - D_y) & -(\omega_z - D_z) \\ (\omega_x - D_x) & 0 & (\omega_z - D_z) & -(\omega_y - D_y) \\ (\omega_y - D_y) & -(\omega_z - D_z) & 0 & (\omega_x - D_x) \\ (\omega_z - D_z) & (\omega_y - D_y) & -(\omega_x - D_x) & 0 \end{bmatrix}\begin{bmatrix} q_0 \\ q_1 \\ q_2 \\ q_3 \end{bmatrix} \tag{30}$$

where first order Gauss-Markov process is considered as gyroscope drift dynamics:

$$\dot{D}_i = -\beta D_i + \sigma\sqrt{2\beta}w(t), \quad i = x, y, z \tag{31}$$

The linearized dynamics (30) and (31) are represented in the following state-space system.

$$\dot{\boldsymbol{x}}^{ah} = \boldsymbol{A}^{ah}\boldsymbol{x}^{ah} + \boldsymbol{G}^{ah}\boldsymbol{u}^{ah} \tag{32}$$

where the ah-superscripts stand for AHRS. The Jacobian matrix, $\boldsymbol{A}^{ah}$ is determined based on Eqs. (30) and (31).

$$\boldsymbol{A}^{ah} = \frac{1}{2}\begin{bmatrix} 0 & -(\omega_x - \boldsymbol{x}_5^{ah}) & -(\omega_y - \boldsymbol{x}_6^{ah}) & -(\omega_z - \boldsymbol{x}_7^{ah}) & \boldsymbol{x}_2^{ah} & \boldsymbol{x}_3^{ah} & \boldsymbol{x}_4^{ah} \\ (\omega_x - \boldsymbol{x}_5^{ah}) & 0 & (\omega_z - \boldsymbol{x}_7^{ah}) & -(\omega_y - \boldsymbol{x}_6^{ah}) & -\boldsymbol{x}_1^{ah} & \boldsymbol{x}_4^{ah} & -\boldsymbol{x}_3^{ah} \\ (\omega_y - \boldsymbol{x}_6^{ah}) & -(\omega_z - \boldsymbol{x}_7^{ah}) & 0 & (\omega_x - \boldsymbol{x}_5^{ah}) & -\boldsymbol{x}_4^{ah} & -\boldsymbol{x}_1^{ah} & \boldsymbol{x}_2^{ah} \\ (\omega_z - \boldsymbol{x}_7^{ah}) & (\omega_y - \boldsymbol{x}_6^{ah}) & -(\omega_x - \boldsymbol{x}_5^{ah}) & 0 & \boldsymbol{x}_3^{ah} & -\boldsymbol{x}_2^{ah} & -\boldsymbol{x}_1^{ah} \\ 0 & 0 & 0 & 0 & -2\beta & 0 & 0 \\ 0 & 0 & 0 & 0 & 0 & -2\beta & 0 \\ 0 & 0 & 0 & 0 & 0 & 0 & -2\beta \end{bmatrix} \tag{33}$$

Eq. (32) is transformed into discrete-time form as:

$$\boldsymbol{x}_{k+1}^{ah} = \boldsymbol{\Phi}_k^{ah}\boldsymbol{x}_k^{ah} + \boldsymbol{w}_k^{ah} \tag{34}$$

where $\boldsymbol{\Phi}_k^{ah}$ is the state transition matrix, and $\boldsymbol{w}_k^{ah}$ is the driven response at time t_{k+1} due to the system noise during the time interval (t_k, t_{k+1}). The covariance matrix associated with $\boldsymbol{w}_k^{ah}$ is obtained as follows.

$$E[\boldsymbol{w}_k^{ah}\boldsymbol{w}_i^{ah}] = \begin{cases} \boldsymbol{Q}_i^{ah}, & i = k \\ 0, & i \neq k \end{cases} \tag{35}$$

Now, the vector matching measurement system is described. Considering the sensed gravity by 3-axis accelerometers, the following gravity vector matching equation between body and reference n-frame coordinates is obtained.

$$\begin{bmatrix} f_x^b \\ f_y^b \\ f_z^b \end{bmatrix} = \begin{bmatrix} \boldsymbol{C}_n^b \end{bmatrix} \begin{bmatrix} 0 \\ 0 \\ -g \end{bmatrix} \tag{36}$$

Eq. (36) is normalized as follows.

$$\frac{1}{norm(\boldsymbol{f}^b)} \begin{bmatrix} f_x^b \\ f_y^b \\ f_z^b \end{bmatrix} = \begin{bmatrix} \boldsymbol{C}_n^b \end{bmatrix} \begin{bmatrix} 0 \\ 0 \\ -1 \end{bmatrix} \tag{37}$$

Therefore, the gravity vector matching based roll and pitch angle are obtained by Eq. (37) as:

$$\begin{aligned} \varphi^{acc} &= a\tan 2(-f_y^b, -f_z^b) \\ \theta^{acc} &= a\sin\left(\frac{f_x^b}{norm(\boldsymbol{f}^b)}\right) \end{aligned} \tag{38}$$

where atan2 represents the four-quadrant version of the arctangent function and asin is the arcsine function. Using Eq. (27), the quaternion measurements are obtained in terms of φ^{acc}, θ^{acc} and ψ^G as:

$$\begin{aligned} q_0^m &= \cos\tfrac{\varphi^{acc}}{2}\cos\tfrac{\theta^{acc}}{2}\cos\tfrac{\psi^G}{2} + \sin\tfrac{\varphi^{acc}}{2}\sin\tfrac{\theta^{acc}}{2}\sin\tfrac{\psi^G}{2} \\ q_1^m &= \sin\tfrac{\varphi^{acc}}{2}\cos\tfrac{\theta^{acc}}{2}\cos\tfrac{\psi^G}{2} - \cos\tfrac{\varphi^{acc}}{2}\sin\tfrac{\theta^{acc}}{2}\sin\tfrac{\psi^G}{2} \\ q_2^m &= \cos\tfrac{\varphi^{acc}}{2}\sin\tfrac{\theta^{acc}}{2}\cos\tfrac{\psi^G}{2} + \sin\tfrac{\varphi^{acc}}{2}\cos\tfrac{\theta^{acc}}{2}\sin\tfrac{\psi^G}{2} \\ q_3^m &= \cos\tfrac{\varphi^{acc}}{2}\cos\tfrac{\theta^{acc}}{2}\sin\tfrac{\psi^G}{2} - \sin\tfrac{\varphi^{acc}}{2}\sin\tfrac{\theta^{acc}}{2}\cos\tfrac{\psi^G}{2} \end{aligned} \tag{39}$$

Now, the measurement equation is defined according to the following discrete form.

$$z_k^{ah} = \boldsymbol{H}_k^{ah}\boldsymbol{x}_k^{ah} + \boldsymbol{e}_k^{ah} \tag{40}$$

where $\boldsymbol{H}_k^{ah}$ is the observation matrix and $\boldsymbol{e}_k^{ah}$ stands for the measurement noise with the following covariance matrix.

$$\begin{aligned} &E[\boldsymbol{e}_k^{ah}\boldsymbol{e}_i^{ah}] = \begin{cases} \boldsymbol{R}_k^{ah}, & i = k \\ 0, & i \neq k \end{cases} \\ &E[\boldsymbol{w}_k^{ah}\boldsymbol{e}_i^{ah}] = 0, \quad \forall i, k \end{aligned} \tag{41}$$

The measurement vector is constructed as follows.

$$\boldsymbol{z}^{ah} = \begin{bmatrix} q_0^m \\ q_1^m \\ q_2^m \\ q_3^m \end{bmatrix} \tag{42}$$

Accordingly, the observation matrix, $\boldsymbol{H}^{ah}$ is obtained as follows.

$$\boldsymbol{H}^{ah} = \begin{bmatrix} 1 & 0 & 0 & 0 & 0 & 0 & 0 \\ 0 & 1 & 0 & 0 & 0 & 0 & 0 \\ 0 & 0 & 1 & 0 & 0 & 0 & 0 \\ 0 & 0 & 0 & 1 & 0 & 0 & 0 \end{bmatrix} \tag{43}$$

Kalman filter is applied as the estimation algorithm in the integrated AHRS. Continuing in a similar estimation procedure as described in Section 2.2, Kalman filter is implemented by two steps as follows.

$$\begin{aligned} \boldsymbol{P}_k^{ah^-} &= \boldsymbol{\Phi}_{k-1}^{ah}\boldsymbol{P}_{k-1}^{ah}\boldsymbol{\Phi}_{k-1}^{ah^T} + \boldsymbol{Q}_{k-1}^{ah} \\ \hat{\boldsymbol{x}}_k^{ah^-} &= \boldsymbol{\Phi}_{k-1}^{ah}\boldsymbol{x}_{k-1}^{ah} \end{aligned} \tag{44}$$

$$\begin{aligned} \boldsymbol{K}_k^{ah} &= \boldsymbol{P}_k^{ah^T}\boldsymbol{H}_k^{ah^T}\left(\mathbf{H_k^{ah}P_k^{ah^-}H_k^{ah^T}}+\mathbf{R_k^{ah}}\right)^{-1} \\ \hat{\boldsymbol{x}}_k^{ah} &= \hat{\boldsymbol{x}}_k^{ah^-}+\boldsymbol{K}_k^{ah}\left(\mathbf{z_k^{ah}}-\mathbf{H_k^{ah}}\hat{\mathbf{x}}_\mathbf{k}^{\mathbf{ah^-}}\right) \\ \boldsymbol{P}_k^{ah} &= \left(\boldsymbol{I}-\boldsymbol{K}_k^{ah}\boldsymbol{H}_k^{ah}\right)\boldsymbol{P}_k^{ah^-} \end{aligned} \tag{45}$$

In the integrated AHRS with GPS, the gyro-based orientation is corrected through the gravity attitude and the GPS heading angle. However, the estimation accuracy of attitude angles will degrade by increase of non-gravitational accelerations on accelerometers due to dynamical maneuvers of vehicle. Therefore, fuzzy adaptive integration of SINS/GPS with AHRS is considered.

4. Fuzzy adaptive integration

In practical applications of low-cost integrated SINS/GPS, orientation accuracy is the main purpose. Although many research works have been already accomplished concerning this issue, the authors focused merely on data fusion and state estimation algorithms. In the current research, a new technique is proposed based on adaptive combination of the SINS/GPS with the AHRS concerning important properties behind the inertial sensing-based orientation determination. The accelerometers provide the gravity-based attitude as the measurement vector of the AHRS estimation filter. However, the gravity attitude is accurate only in stationary or quasi-stationary maneuvres of carrying vehicle. On the other hand, though the gyro-based orientation is determined independent of kinematical and dynamical maneuvers, its integrating structure yields time increasing measurement errors and large orientation drifts.

According to the above explanations, the integrated AHRS system provides more accurate orientation estimation in stationary or quasi-stationary motions compared to conventional SINS/GPS system. Therefore, in stationary maneuvering conditions, the AHRS data is utilized to improve the performance of the SINS/GPS system. To acquire this aim, prior to any decision, the maneuvering level during the vehicle motion should be properly determined. When the imposed non-gravitational acceleration is negligible, the AHRS data should be dominant in the final combined orientation data. However, in the high-accelerated conditions, the AHRS accuracy decreases and thus the integrated orientation should place more weight on the SINS/GPS data.

The principles of fuzzy logic are applied to construct an intelligent algorithm for decision-making between the SINS/GPS and the AHRS. The fuzzy logic is considered mainly because of its simplicity and global merging capabilities. Expert knowledge is used to characterize inputs and outputs and connect them by a set of inference rules [22]. The basic idea behind the technique is to evaluate the maneuvering level during the vehicle motion through the inertial sensors measurements. Accordingly, the inputs to the fuzzy inference system are defined as follows.

$$\begin{aligned} \eta_1 &= |norm(mean_N(\boldsymbol{f}^n)) - norm(\boldsymbol{g}^n)| \\ \eta_2 &= norm(mean_N(\boldsymbol{\omega}_{ib}^b)) \end{aligned} \tag{46}$$

where $mean_N(\cdot)$ denote the mean value for every N-sample. If the sampling time is characterized by Δt, the inputs are updated every $N \times \Delta t$ seconds. Mamdani-type fuzzy inference system combines the input data of Eq. (46) to make an intelligent decision between the AHRS and the SINS/GPS results. Two weighting coefficients, ξ_1 (for SINS/GPS data) and ξ_2 (for AHRS data) are considered as the outputs of fuzzy system. Block diagram of Fig. 2 shows the main structure of the fuzzy inference system developed for the aforementioned decision-making.

During the fuzzification process, the system inputs are rated in terms of their belongingness to a pre-specified membership function. Hereby, the inputs are converted from crisp variables to fuzzy linguistic variables. In fuzzy inference engine, a set of rule-base are acquired for the functioning of the predefined adaptive integration scheme. The fuzzy outputs of the

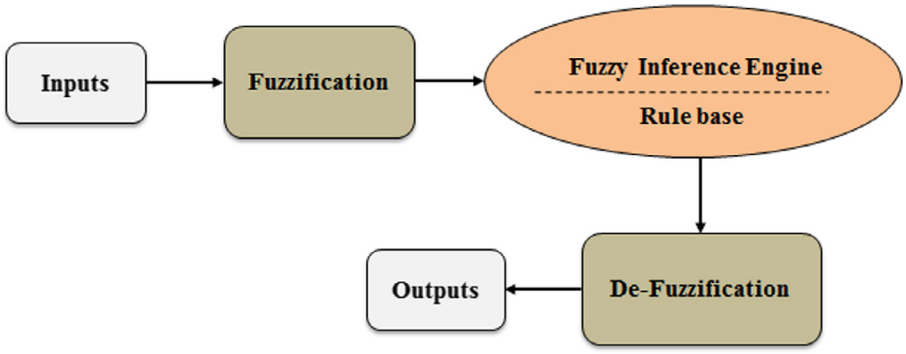

Fig. 2. The main structure of the fuzzy inference system.

fuzzy inference engine are de-fuzzified in the de-fuzzification process. Accordingly, the weighting coefficients named as ξ_1 and ξ_2 are determined. Fuzzy logic approach is implemented based on linguistic IF (antecedent), THEN (consequent) rules. The antecedents and the consequents variables are corresponded to fuzzy sets of $\eta_i \in \underset{\sim}{\mathrm{A}}_{ir}^{l}$ and $\xi_j \in \underset{\sim}{\mathrm{C}}_{jr}^{l}$, respectively. By fuzzy sets, $\underset{\sim}{\mathrm{A}}_{ir}^{l}$ and $\underset{\sim}{\mathrm{C}}_{jr}^{l}$, i and j denote the numbers of input and output fuzzy sets, respectively. Moreover, r is the rule-number and l is a linguistic label that specifies membership function associating to each fuzzy set. Therefore, $\mu_{\underset{\sim}{\mathrm{A}}_{ir}^{l}}(\eta_i)$ and $\mu_{\underset{\sim}{\mathrm{C}}_{jr}^{l}}(\xi_j)$ stand for the membership degree of antecedent and consequent variables. For example, the symbol $\mu_{\underset{\sim}{\mathrm{A}}_{ir}^{l}}(\eta_i)$ is the membership degree of element η_i in the membership function of fuzzy set $\underset{\sim}{\mathrm{A}}_{ir}^{l}$. In other words, $\mu_{\underset{\sim}{\mathrm{A}}_{ir}^{l}}(\eta_i)$ is a normal value in the interval [0, 1] to measure the degree which element η_i belongs to fuzzy set $\underset{\sim}{\mathrm{A}}_{ir}^{l}$.

On the basis of aforementioned adaptive strategy for combination of SINS/GPS and AHRS, the fuzzy inference system is implicated using three fuzzy sets, *S*, *M* and *L* that stand for small, medium and large, respectively. Based on the knowledge and the experience of expert engineers in the navigation field, the following fuzzy rule-base including 9 rules is defined to construct the fuzzy adaptive integration scheme.

$$
\begin{aligned}
&\text{Rule1}: \ IF \mu_{\underset{\sim}{\mathrm{A}}_{11}^{L}}(\eta_1) \ and \ \mu_{\underset{\sim}{\mathrm{A}}_{21}^{L}}(\eta_2) \ THEN \ \mu_{\underset{\sim}{\mathrm{C}}_{11}^{L}}(\xi_1), \mu_{\underset{\sim}{\mathrm{C}}_{21}^{S}}(\xi_2)\\
&\text{Rule2}: \ IF \mu_{\underset{\sim}{\mathrm{A}}_{12}^{L}}(\eta_1) \ and \ \mu_{\underset{\sim}{\mathrm{A}}_{22}^{M}}(\eta_2) \ THEN \ \mu_{\underset{\sim}{\mathrm{C}}_{12}^{L}}(\xi_1), \mu_{\underset{\sim}{\mathrm{C}}_{22}^{S}}(\xi_2)\\
&\text{Rule3}: \ IF \mu_{\underset{\sim}{\mathrm{A}}_{13}^{L}}(\eta_1) \ and \ \mu_{\underset{\sim}{\mathrm{A}}_{23}^{S}}(\eta_2) \ THEN \ mu_{\underset{\sim}{\mathrm{C}}_{13}^{M}}(\xi_1), \mu_{\underset{\sim}{\mathrm{C}}_{23}^{S}}(\xi_2)\\
&\text{Rule4}: \ IF \mu_{\underset{\sim}{\mathrm{A}}_{14}^{M}}(\eta_1) \ and \ \mu_{\underset{\sim}{\mathrm{A}}_{24}^{L}}(\eta_2) \ THEN \ \mu_{\underset{\sim}{\mathrm{C}}_{14}^{M}}(\xi_1), \mu_{\underset{\sim}{\mathrm{C}}_{24}^{S}}(\xi_2)\\
&\text{Rule5}: \ IF \mu_{\underset{\sim}{\mathrm{A}}_{15}^{M}}(\eta_1) \ and \ \mu_{\underset{\sim}{\mathrm{A}}_{25}^{M}}(\eta_2) \ THEN \ \mu_{\underset{\sim}{\mathrm{C}}_{15}^{M}}(\xi_1), \mu_{\underset{\sim}{\mathrm{C}}_{25}^{M}}(\xi_2)\\
&\text{Rule6}: \ IF \mu_{\underset{\sim}{\mathrm{A}}_{16}^{M}}(\eta_1) \ and \ \mu_{\underset{\sim}{\mathrm{A}}_{26}^{S}}(\eta_2) \ THEN \ \mu_{\underset{\sim}{\mathrm{C}}_{16}^{M}}(\xi_1), \mu_{\underset{\sim}{\mathrm{C}}_{26}^{M}}(\xi_2)\\
&\text{Rule7}: \ IF \mu_{\underset{\sim}{\mathrm{A}}_{17}^{S}}(\eta_1) \ and \ \mu_{\underset{\sim}{\mathrm{A}}_{27}^{S}}(\eta_2) \ THEN \ \mu_{\underset{\sim}{\mathrm{C}}_{17}^{S}}(\xi_1), \mu_{\underset{\sim}{\mathrm{C}}_{27}^{L}}(\xi_2)\\
&\text{Rule8}: \ IF \mu_{\underset{\sim}{\mathrm{A}}_{18}^{S}}(\eta_1) \ and \ \mu_{\underset{\sim}{\mathrm{A}}_{28}^{M}}(\eta_2) \ THEN \ \mu_{\underset{\sim}{\mathrm{C}}_{18}^{S}}(\xi_1), \mu_{\underset{\sim}{\mathrm{C}}_{28}^{L}}(\xi_2)\\
&\text{Rule9}: \ IF \mu_{\underset{\sim}{\mathrm{A}}_{19}^{S}}(\eta_1) \ and \ \mu_{\underset{\sim}{\mathrm{A}}_{29}^{L}}(\eta_2) \ THEN \ \mu_{\underset{\sim}{\mathrm{C}}_{19}^{S}}(\xi_1), \mu_{\underset{\sim}{\mathrm{C}}_{29}^{M}}(\xi_2)
\end{aligned}
\tag{47}
$$

When the inputs of the fuzzy inference system are near to zero, the vehicle is in a stationary or quasi-stationary mode. In contrary, increasing in the magnitude of the inputs means that the vehicle is undergoing dynamic maneuvering and non-gravitational acceleration. Figs. 3 and 4 show the membership functions of the fuzzy sets designed by use of expert knowledge and real test results.

Using the min T-norm operator for the antecedent part of the fuzzy rules, the combined membership value is obtained for each rule as follows.

$$
\mu_{\underset{\sim}{\mathrm{A}}}^{r}(\eta_1, \eta_2) = \min(\mu_{\underset{\sim}{\mathrm{A}}_{1r}^{l}}(\eta_1), \mu_{\underset{\sim}{\mathrm{A}}_{2r}^{l}}(\eta_2)) \quad for \ r = 1, 2, \ldots, 9 \tag{48}
$$

The fuzzy rules are individually inferred through Mamdani's minimum engine to calculate the overall fuzzy value for each rule output [23].

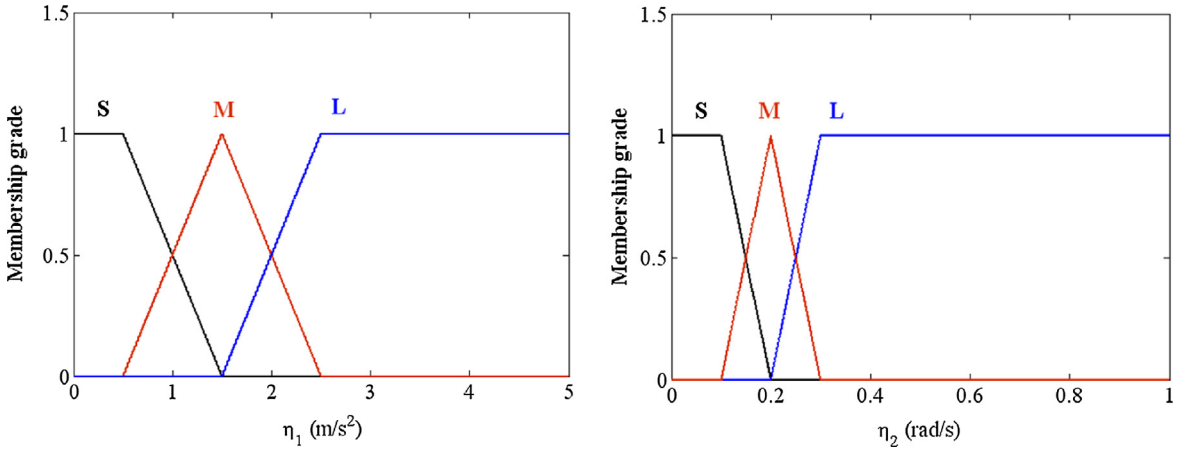

Fig. 3. Membership function of input variables.

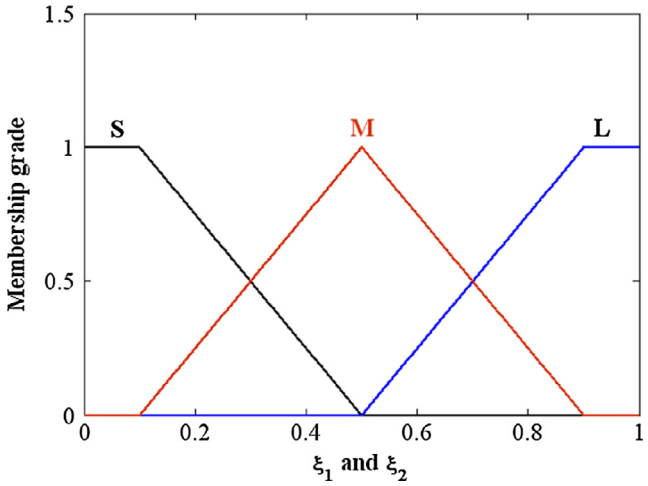

Fig. 4. Membership function of output variables.

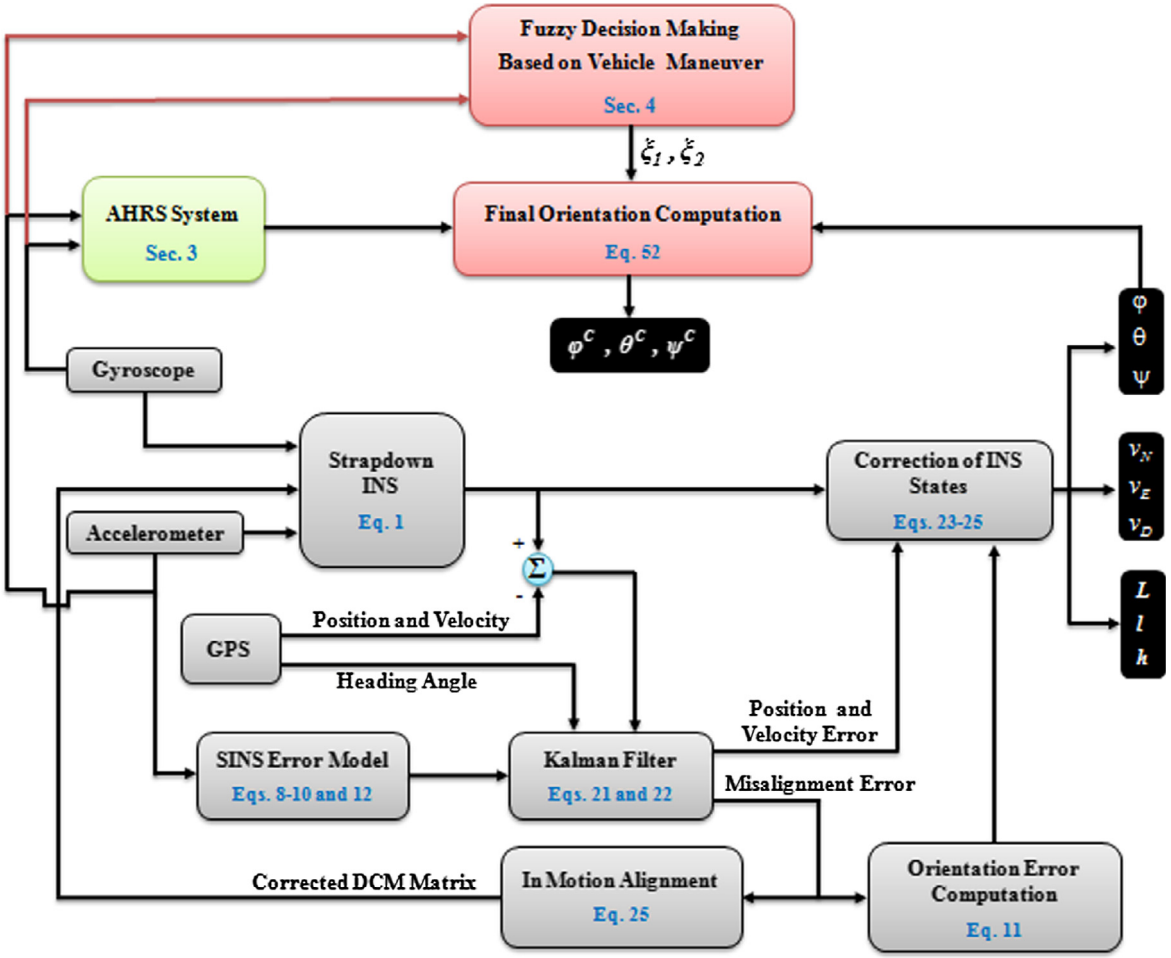

Fig. 5. Block diagram of proposed adaptive integration scheme.

$$\mu_{\underset{\sim}{C}}^{r}(\xi_1) = \min(\mu_{\underset{\sim}{C}}^{r}(\eta_1,\eta_2), \mu_{\underset{\sim}{C}_{1r}^{l}}(\xi_1)) \quad for\ r = 1,2,\ldots,9$$
$$\mu_{\underset{\sim}{C}}^{r}(\xi_2) = \min(\mu_{\underset{\sim}{C}}^{r}(\eta_1,\eta_2), \mu_{\underset{\sim}{C}_{2r}^{l}}(\xi_2)) \quad for\ r = 1,2,\ldots,9 \tag{49}$$

Using the max S-norm operator on the fuzzy rules outputs, the following aggregated/global fuzzy outputs are obtained.

$$\mu_{\underset{\sim}{C}}(\xi_1) = \max_{r=1}^{n_r}(\mu_{\underset{\sim}{C}}^{r}(\xi_1))$$
$$\mu_{\underset{\sim}{C}}(\xi_2) = \max_{r=1}^{n_r}(\mu_{\underset{\sim}{C}}^{r}(\xi_2)) \tag{50}$$

where n_r represents the number of fired rules in the fuzzy rule-base with non-zero outputs. Finally, the global fuzzy outputs are transformed in crisp values based on the centroid de-fuzzification method as follows [24].

Table 2
Specification of inertial sensor of ADIS-16407.

Parameter	Gyro	Accelerometer
Misalignment (axis-to-frame)	0.05 deg	0.2 deg
Misalignment (axis-to-axis)	0.5 deg	0.5 deg
Initial bias error (1σ)	3 deg/s	50 mg
In-run bias stability (1σ)	0.007 deg/s	0.2 mg
Random walk (1σ)	1.9 deg/$\sqrt{}$h	0.2 m/s/$\sqrt{}$h
Output noise (no filtering)	0.8 deg/s rms	9 mg rms
Dynamic range	±300 deg/s	±18 g

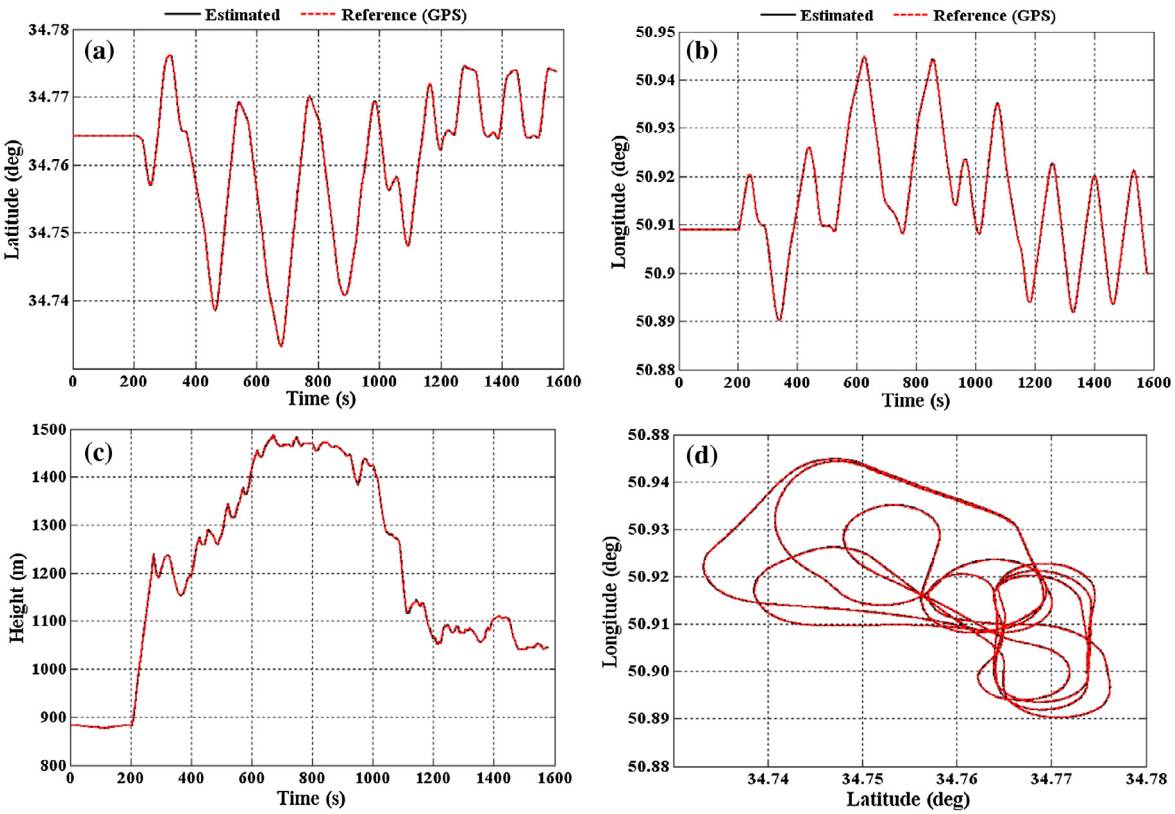

Fig. 6. Estimation results of position components compared with GPS data.

$$\xi_1^* = \frac{\int \mu_{\tilde{\zeta}}(\xi_1)\cdot\xi_1 d\xi_1}{\int \mu_{\tilde{\zeta}}(\xi_1) d\xi_1}$$
$$\xi_2^* = \frac{\int \mu_{\tilde{\zeta}}(\xi_2)\cdot\xi_2 d\xi_2}{\int \mu_{\tilde{\zeta}}(\xi_2) d\xi_2} \tag{51}$$

Using the fuzzy weighting coefficients, ξ_1^* and ξ_1^*, the aggregated orientation estimation is computed in accordance with the following equation.

$$\text{Orientation} = \frac{\xi_1^* \cdot (\text{SINS/GPS Orientation}) + \xi_2^* \cdot (\text{AHRS Orientation})}{\xi_1^* + \xi_2^*} \tag{52}$$

The complete block-diagram of the proposed adaptive integration scheme is depicted in Fig. 5. As shown in Fig. 5, the proposed integrated inertial navigation scheme consists three main parts comprising SINS/GPS, AHRS and fuzzy inference system. There exists no direct measurement for attitude estimation in the filter algorithm of the SINS/GPS section. However, in the AHRS section the sensed gravity by the accelerometers provides accurate attitude measurements in the stationary or quasi-stationary motions.

The motion modes are detected by fuzzy intelligent system to make more accurate orientation by the AHRS and the SINS/GPS. Furthermore, the fuzzy inference system provides efficient combination of the SINS/GPS and the AHRS data to enhance the overall navigation accuracy.

5. Experimental results and discussion

The accuracy of the proposed adaptive integration scheme has been evaluated using experimental results collected from airborne test. The MEMS-grade inertial sensors of low-cost ADIS-16407 IMU are used to generate inertial data comprising the angular rates and the specific forces. Garmin-35 GPS receiver has been used to produce the measurement data for the

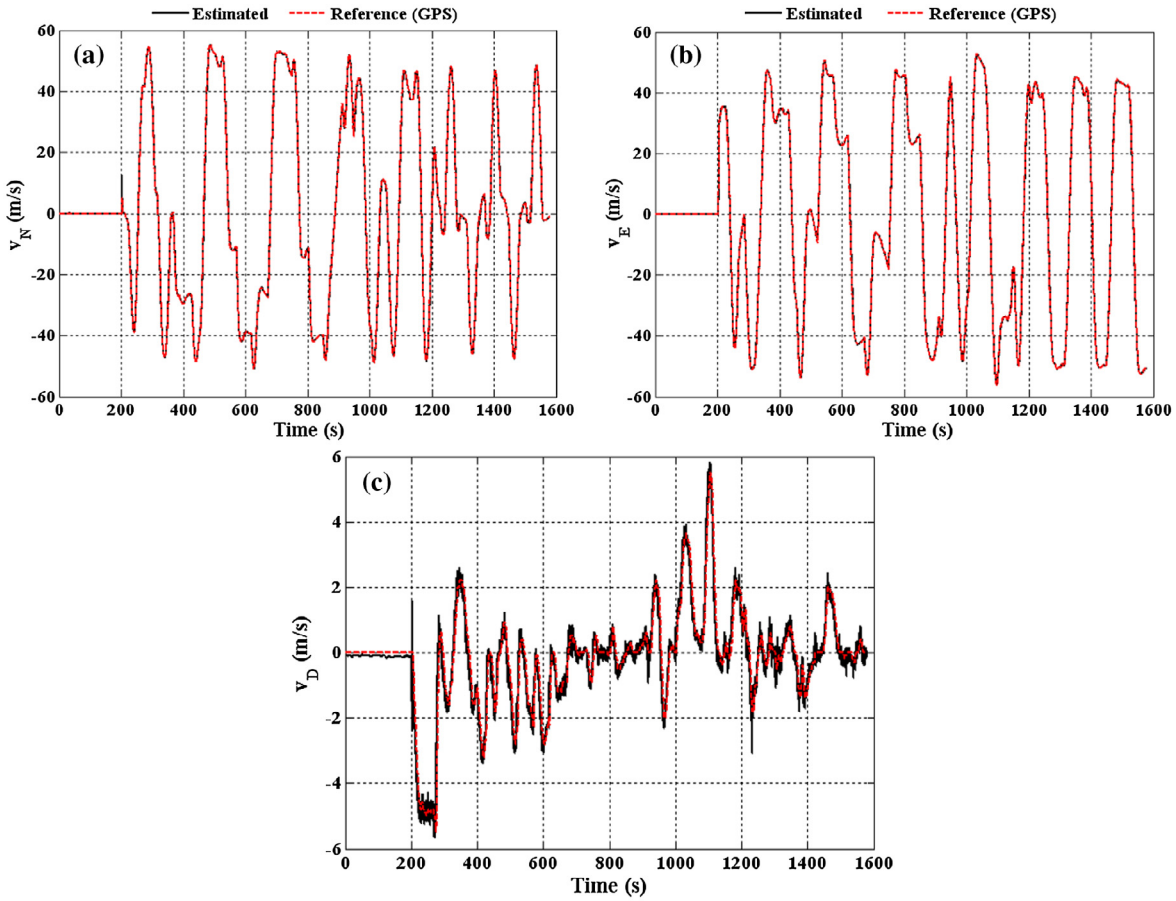

Fig. 7. Estimation results of velocity components compared with GPS data.

integrated navigation system. The main statistical specifications of the inertial sensors of ADIS-16407 IMU are given in Table 2.

In the flight test, the IMU was installed beside a precise Vitans integrated navigation system. The highly accurate attitude data provided from Vitans system has been considered as the reference values for the attitude accuracy assessment of the proposed algorithm. The raw IMU measurements are acquired at a sampling rate of 50 Hz. The SINS orientation, velocity and position are delivered at the same rate, but corrected by the GPS data at a rate of 1 Hz inside the Kalman filter. The flight test has been executed for approximately 1600 s along a trajectory with wide range dynamic maneuvers. Fig. 6 illustrates the results obtained for the position estimation during the flight test.

During the overall 26.5 min interval, the system works 200 s in the initial alignment regime in which the vehicle is in stationary mode. In the initial alignment regime, the attitude and heading angles are initialized using accelerometer outputs and magnetometers, respectively. Additionally, the on-off bias of the gyroscope is compensated. Vehicle dynamics and maneuvering can be observed via the motion trajectory in the horizontal plane as illustrated in Fig. 6(d). The position components estimated by the proposed algorithm have been compared with those of the GPS system. The estimated values of the velocity components are represented in Fig. 7.

Figs. 6 and 7 exhibit the good performance of the proposed algorithm in position and velocity estimation. For better evaluation, the statistical analysis by the mean and the standard deviation values of the position and the velocity estimation errors are gathered in Table 3.

To further validate the performance of the proposed approach, the results are compared with those of an artificial intelligence-based INS/GPS system in which input-delayed adaptive neuro-fuzzy inference system (IDANFIS) has been used for data fusion. A comprehensive description was presented in [11]. As discussed in [11], the proposed IDANFIS approach was evaluated in vehicular field test in which MEMS-grade MIDG-II IMU was used to provide inertial measurements. The results presented in [11] shows that the mean values of the position error and velocity error are about 0.41 m and 0.13 m/s, respectively. By comparing these results with the statistical information of Table 3, the performance of the proposed fuzzy adaptive integration scheme is clearly validated.

The estimation results of the attitude and heading angles are shown in Figs. 8–10. To legitimize the performance assessment of the presented integrated navigation algorithm, the results are compared with those of the conventional integration scheme. The conventional scheme contains a standard Kalman filter algorithm implemented on the SINS dynamics. The atti-

Table 3
Mean values and standard deviation of the position and velocity estimation error.

Navigation parameter	Mean value of estimation error	Standard deviation of estimation error ($\pm 1\sigma$)
V-north (m/s)	−0.01532	0.6347
V-east (m/s)	−0.01762	0.6273
V-down (m/s)	−0.05910	0.3800
Latitude (m)	0.03673	9.0710
Longitude (m)	0.06946	12.080
Altitude (m)	0.06354	1.4810

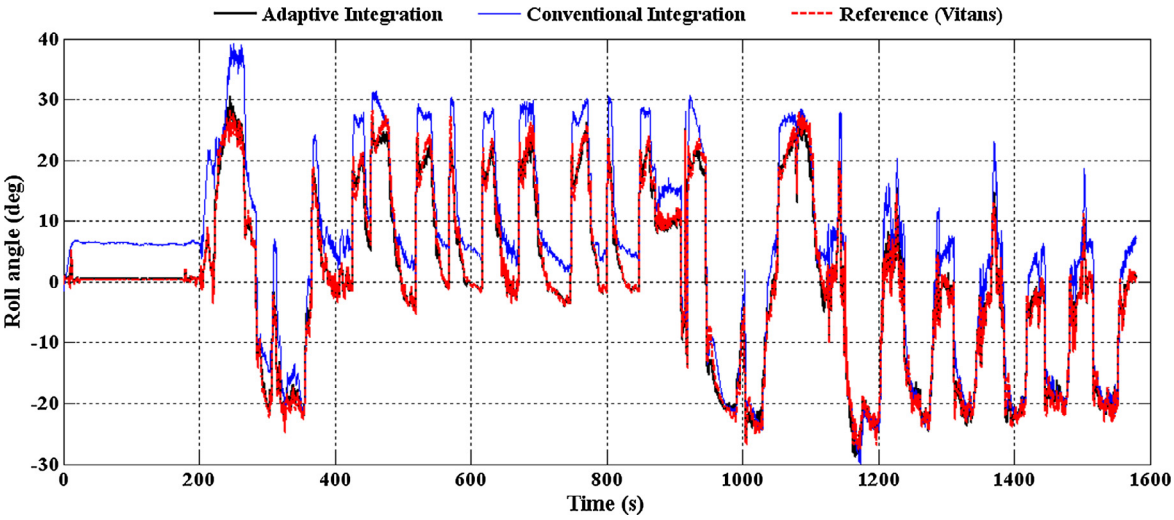

Fig. 8. Estimation result of roll angle compared with reference value of Vitans system.

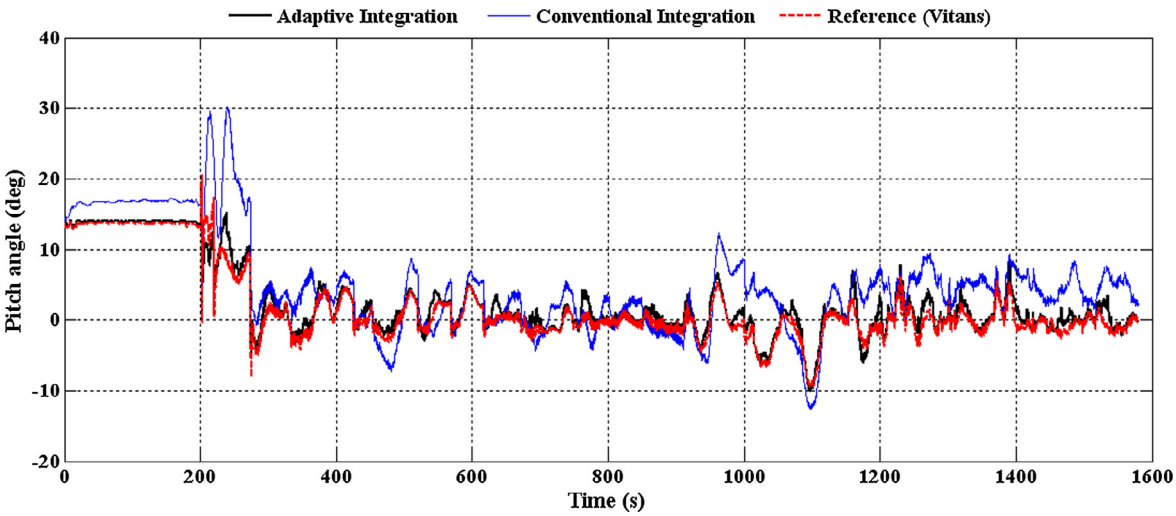

Fig. 9. Estimation result of pitch angle compared with reference value of Vitans system.

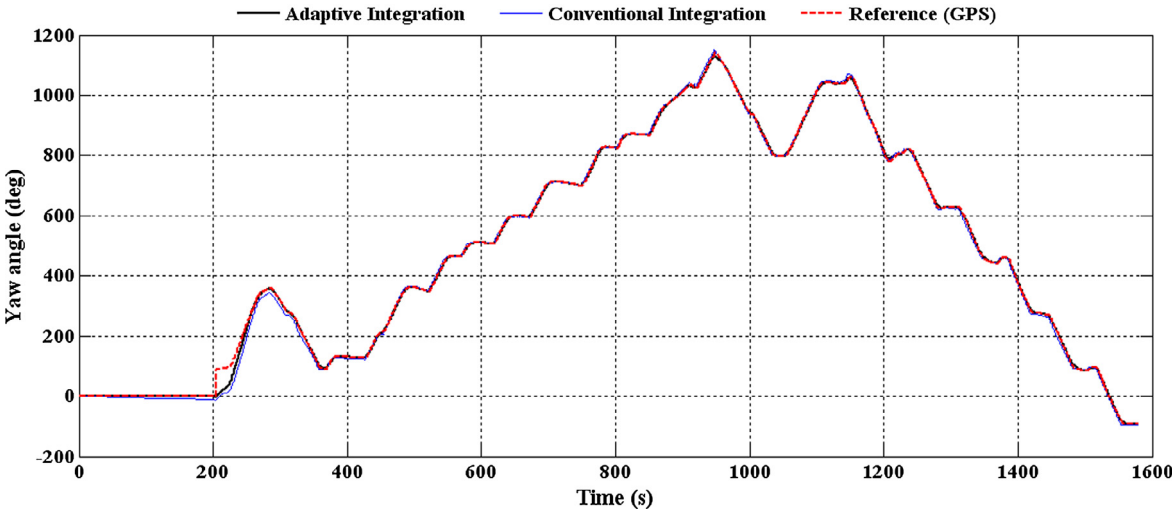

Fig. 10. Estimation result of the yaw angle compared with the reference value of GPS system.

tude angles of the highly accurate Vitans system as well as the GPS heading angle have been considered as the reference values of the orientation components.

As shown in Figs. 8–10, the proposed fuzzy adaptive integration scheme results in better accuracy in comparison to the conventional integration scheme, particularly in the attitude estimation. During non-accelerated maneuvers in quasi-stationary mode, the vector matching between the accelerometer-sensed gravity and the reference gravity in Eq. (37) provide more accurate measurements for the attitude estimation. As the main advantage, the proposed adaptive integration scheme benefits from the accurate gravity attitude in quasi-stationary motions. In contrary, as the vehicle undergoes

Table 4
Mean values and standard deviation of orientation estimation error.

Navigation parameter	Conventional integration scheme		Proposed integration scheme	
	Mean value of estimation error	Standard deviation of estimation error ($\pm 1\sigma$)	Mean value of estimation error	Standard deviation of estimation error ($\pm 1\sigma$)
Roll (deg)	3.971	3.148	−0.0839	1.015
Pitch (deg)	2.912	3.584	0.6562	0.986
Yaw (deg)	0.039	5.729	−0.0176	2.834

non-gravitational accelerations, considerable error may be produced by the vector matching of Eq. (37). In these situations, gravity attitude cannot provide appropriate measurements for the state estimation filter. In the proposed adaptive integration scheme, fuzzy inference system makes an appropriate decision based on the vehicle maneuvers to optimize the performance of the integrated navigation system, especially in the orientation estimation. Unlike switch-based approach in which the switching may lead to abrupt change in the estimated results, the proposed fuzzy adaptive integration yields more smooth results. In other words, the overall estimation accuracy is not sensitive to the interference between the AHRS and the SINS/GPS results. The statistical analysis comprising of mean and standard deviation values of the orientation estimation error corresponding to both the conventional and the proposed adaptive integration schemes are gathered in Table 4.

As illustrated in Table 4, using the proposed adaptive integration scheme, the mean and the standard deviation values of the orientation estimation error have been considerably decreased.

6. Conclusions

The paper specifically dealt with the orientation estimation problem in low-cost SINS/GPS integrated navigation system. The main concept behind the proposed integrated navigation system is that the gravity attitude obtained from the accelerometer can provide valuable measurement data for state estimation filter in the low-cost inertial integrated navigation systems. Certainly, when the external acceleration was increased, the gravity attitude could not bring about relatively accurate measurement as in the stationary or quasi-stationary mode. In the paper, an adaptive integration scheme has been designed to utilize the gravity attitude in the inertial navigation, appropriately. Mamdani-type fuzzy inference system has been developed to construct the adaptive integration scheme. Using knowledge-based fuzzy logic, the inertial measurements are analysed and the dynamics regime of the motion is determined. Accordingly, the accelerometer outputs are intelligently utilized in the integration scheme to achieve higher accuracy of orientation estimation. On average, the proposed algorithm decreased the mean and the standard deviation of the orientation estimation error from 2.307 deg and 4.154 deg in conventional SINS/GPS to 0.253 deg and 1.612 deg, respectively. Considering the theoretical and practical superiorities compared to traditional standard algorithms, the proposed integration scheme is more suitable for implementation in low-cost integrated inertial navigation systems.

Appendix A. Supplementary material

Supplementary data associated with this article can be found, in the online version, at http://dx.doi.org/10.1016/j.ymssp.2017.06.030.

References

[1] K.T. Leung et al, Road vehicle state estimation using low-cost GPS/INS, Mech. Syst. Sign. Process. 25 (6) (2011) 1988–2004.
[2] M.S. Grewal, L.R. Weill, A.P. Andrews, Global Positioning Systems, Inertial Navigation, and Integration, John Wiley & Sons, 2007.
[3] Y. Kubo et al, Nonlinear filtering methods for the INS/GPS in-motion alignment and navigation, Int. J. Innov. Comput. Inf. Control 2 (2006) 1137–1151.
[4] W. Wang, Z.-Y. Liu, R.-R. Xie, Quadratic extended Kalman filter approach for GPS/INS integration, Aerosp. Sci. Technol. 10 (8) (2006) 709–713.
[5] P. Doostdar, J. Keighobadi, Design and implementation of SMO for a nonlinear MIMO AHRS, Mech. Syst. Sign. Process. 32 (2012) 94–115.
[6] Q. Li, Y. Ben, F. Sun, A novel algorithm for marine strapdown gyrocompass based on digital filter, Measurement 46 (1) (2013) 563–571.
[7] H. Milanchian, J. Keighobadi, H. Nourmohammadi, Magnetic calibration of three-axis strapdown magnetometers for applications in MEMS attitude-heading reference systems, Amirkabir Int. J. Model. Identificat. Simul. Control 47 (1) (2015) 55–65.
[8] M.A. Jaradat, M.F. Abdel-Hafez, Non-Linear autoregressive delay dependent INS/GPS davigation system using neural networks, IEEE Sens. J. 17 (4) (2017) 1105–1115.
[9] H. Nourmohammadi, J. Keighobadi, Decentralized INS/GPS system with MEMS-grade inertial sensors using QR-factorized CKF, IEEE Sens. J. 17 (11) (2017) 3278–3287, http://dx.doi.org/10.1109/JSEN.2017.2693246.
[10] D. Petković et al, Adaptive neuro-fuzzy maximal power extraction of wind turbine with continuously variable transmission, Energy 64 (2014) 868–874.
[11] K. Saadeddin et al, Performance enhancement of low-cost, high-accuracy, state estimation for vehicle collision prevention system using ANFIS, Mech. Syst. Sign. Process. 41 (1) (2013) 239–253.
[12] M. Kyrarini, S. Slavnić, D. Ristić-Durrant, Fuzzy controller for the control of the mobile platform of the CORBYS robotic gait rehabilitation system, Facta Univers., Ser.: Mech. Eng. 12 (3) (2014) 223–234.
[13] D. Petković, M. Gocić, S. Shamshirband, Adaptive neuro-fuzzy computing technique for precipitation estimation, Facta Univ., Ser.: Mech. Eng. 14 (2) (2016) 209–218.
[14] D. Petković, Ž. Ćojbašič, V. Nikolić, Adaptive neuro-fuzzy approach for wind turbine power coefficient estimation, Renew. Sustain. Energy Rev. 28 (2013) 191–195.
[15] N. Musavi, J. Keighobadi, Adaptive fuzzy neuro-observer applied to low cost INS/GPS, Appl. Soft Comput. 29 (2015) 82–94.
[16] B. Boada, M. Boada, V. Diaz, Vehicle sideslip angle measurement based on sensor data fusion using an integrated ANFIS and an unscented Kalman filter algorithm, Mech. Syst. Sign. Process. 72 (2016) 832–845.
[17] K.J. Walchko et al., Embedded low cost inertial navigation system, in: Florida Conference on Recent Advances in Robotics, FAU, Dania Beach, FL, May, 2003.
[18] R.M. Rogers, Applied Mathematics in Integrated Navigation Systems, vol. 1, AIAA, 2003.
[19] S. Nassar et al, Modeling inertial sensor errors using autoregressive (AR) models, Navigation 51 (4) (2004) 259–268.
[20] C.D. Petersen et al, A Kalman filter approach to virtual sensing for active noise control, Mech. Syst. Sign. Process. 22 (2) (2008) 490–508.
[21] D. Titterton, J.L. Weston, Strapdown Inertial Navigation Technology, vol. 17, IET, 2004.
[22] A.H. Ali et al, DFLC: dynamic fuzzy logic controller for intrusion detection, Facta Univ., Ser.: Mech. Eng. 12 (2) (2014) 183–193.
[23] J. Keighobadi, Fuzzy calibration of a magnetic compass for vehicular applications, Mech. Syst. Sign. Process. 25 (6) (2011) 1973–1987.
[24] T.J. Ross, Fuzzy Logic with Engineering Applications, John Wiley & Sons, 2009.